

# Hyperbolic formulations and numerical relativity: Experiments using Ashtekar's connection variables\*

Hisaki Shinkai<sup>†</sup>

*Center for Gravitational Physics and Geometry, 104 Davey Lab., Department of Physics,  
The Pennsylvania State University, University Park, Pennsylvania 16802-6300, USA*

Gen Yoneda<sup>‡</sup>

*Department of Mathematical Sciences, Waseda University, Shinjuku, Tokyo, 169-8555, Japan  
(May 1, 2000)*

In order to perform stable long-time numerical integration of the Einstein equation, several hyperbolic systems have been proposed. We here present our numerical comparisons between weakly hyperbolic, strongly hyperbolic, and symmetric hyperbolic systems based on Ashtekar's connection variables. The primary advantage for using this connection formulation in this experiment is that we can keep using the same dynamical variables for all levels of hyperbolicity. Our numerical code demonstrates gravitational wave propagation in plane symmetric spacetimes, and we compare “the stability” by monitoring the violation of the constraints. By comparing the results obtained from the weakly hyperbolic system, we observe the strongly and symmetric hyperbolic system show better stability properties, but not so much difference between the latter two. Rather, we find that the symmetric hyperbolic system is not always the best for controlling stability. Similar conclusions are obtained also in the Maxwell system.

This study is the premier for presenting full numerical simulations using Ashtekar's variables. We also describe our procedures in detail.

## I. INTRODUCTION

Numerical relativity – solving the Einstein equation numerically – is now one of the essential field in gravity researches. As is well known, the critical collapse in gravity system was first discovered by numerical simulation [1]. The current main stream of numerical relativity is to demonstrate final phase of the compact binary objects related to gravitational wave observations [2], and the efforts are now again shedding lights on the mathematical structure of the Einstein equations.

Up to a couple years ago, Arnowitt-Deser-Misner (ADM) decomposition of the Einstein equation was taken as the standard formulation for numerical relativists. Difficulties in stable long-term evolutions were supposed to be overcome by choosing proper gauge conditions and boundary conditions. Recently, however, several numerical experiments show that ADM is not the best formulation for numerics, and finding a better formulation becomes one of the main research topics.

One direction in the community is to apply conformally decoupled and tracefree re-formulation of ADM system which were first used by Nakamura *et al.* [3]. The usefulness of this re-formulation were confirmed by another groups to show a long-term stability <sup>1</sup> [4,5]. Although there is an effort to show why this re-formulation is better than ADM [6], we do not yet know this method is robust for all situations.

Another alternative approaches to ADM is to formulate Einstein equations as they reveal hyperbolicity [7]. A certain kind of hyperbolicity of the dynamical equations are essential to analyze their propagation features mathematically, and are known to be useful in numerical approximations (we explain these points in §2). The propagation of the original ADM constraint equations obeys well-posed behavior [8] but dynamical equations of ADM system is not hyperbolic system at all (and these facts can be also applied to the conformally decoupled version). Several hyperbolic formulations are so far proposed to express the Einstein equation, with different levels: weakly, strongly and symmetric hyperbolic systems (we will discuss in detail in §2). Several numerical tests were also performed in this direction, and we can see advantages in numerical stability than original ADM system (e.g. tests [9] of Bona-Massó's flux conservative form [10], tests [11] of Choquet-Bruhat and York (95)'s symmetrizable form [12]), but also a coordinate

---

\*gr-qc/0005003

<sup>1</sup>We use the word ‘stability’ hereafter indicating the less violation of the constraints during the free numerical evolution of the initial data. Here free evolution means that we only solve the constraints on the initial hypersurface.

shock capturing feature is reported ([13] in the system of [9]). Or a symmetric hyperbolic system of [14] is numerically studied in the so-called “conformal Einstein” approach [15].

The following questions, therefore, naturally come up to us (cf. [16]): (1) Does hyperbolicity actually contribute the numerical stability? (2) If so, which level of hyperbolic formulation is practically useful for numerical applications? (or does the symmetric hyperbolicity solve all the difficulties?) (3) Is there any other approaches to improve the stabilities of the system?

In this paper, we try to answer these questions from our simple numerical experiments. Such comparison is suitable when the fundamental equations cast on the same interface, and that is available at this moment only using Ashtekar’s connection variables [17,18]. More precisely, the authors’ recent studies showed the followings: (a) the original set of dynamical equations proposed by Ashtekar forms already a weakly hyperbolic system [19], (b) by requiring additional gauge condition *or* adding constraints to the dynamical equations, we can obtain a strongly hyperbolic system [19], (c) by requiring additional gauge condition *and* adding constraints to the dynamical equations, we can obtain symmetric hyperbolic system [19,20], and finally (d) based on the above symmetric hyperbolic system, we can construct a set of dynamical system which is robust for perturbative errors for constraints and reality conditions [21] (*aka.*  $\lambda$ -system [22]).

Based on the above results (a)-(c), we developed our numerical code which handles gravitational wave propagation problem in the plane symmetric spacetime. We performed the time evolutions using the above three-levels of Ashtekar’s dynamical equations together with the standard ADM equation. We compare these stability by monitoring the violation of the constraints. We also show the demonstrations of our  $\lambda$ -system (above (d)) in our succeeding paper (Paper II) [41], together with new proposal for controlling the stability.

It is worth remarking that this study is the first one which shows full numerical simulations of Lorentzian spacetime using Ashtekar’s connection variables. This research direction was suggested just after Ashtekar completed his formulation [23], but has not yet been done. Historically, an application to numerical relativity of the connection formulation was also suggested [18,24] to use Capovilla-Dell-Jacobson’s version of connection variables [25], which produce a direct relation to Newman-Penrose’s  $\Psi$ s. However, here, we apply Ashtekar’s original formulation, because we know how to treat its reality condition in detail [26,27]. We will also describe the basic numerical procedures in this paper.

The outline of this paper is following. In the next section, we review the mathematical background of hyperbolic formulation briefly and display our fundamental dynamical equations. In §III, we describe our numerical procedures. We present our experiments in §IV and §V, and summarize them in §VI. The Appendix A is for showing Ashtekar’s basic equations in our notation, and we also present our experiments based on the Maxwell equation in the Appendix B.

## II. HYPERBOLIC FORMULATIONS

### A. definitions, properties, mathematical backgrounds

We say that the system is a first-order (quasi-linear) partial differential equation system, if a certain set of (complex-valued) variables  $u_\alpha$  ( $\alpha = 1, \dots, n$ ) forms

$$\partial_t u_\alpha = \mathcal{M}^{l\beta}{}_\alpha(u) \partial_l u_\beta + \mathcal{N}_\alpha(u), \quad (2.1)$$

where  $\mathcal{M}$  (the characteristic matrix) and  $\mathcal{N}$  are functions of  $u$  but do not include any derivatives of  $u$ . If the characteristic matrix is a Hermitian matrix, then we say (2.1) is a symmetric hyperbolic system.

To write the system in the hyperbolic form is the essential process to prove the system is well-posed. Here, the well-posedness means that the solution of the system is proven to be its (1°) existence (of at least one solution  $u$ , (2°) uniqueness (i.e., either one or zero solutions), and (3°) stability (often called continuous dependence of solutions  $\{u\}$  upon the Cauchy data). The Cauchy problem under weak hyperbolicity is not, in general,  $C^\infty$  well-posed. The symmetric hyperbolic system gives us the energy integral inequalities which are the primary tools for studying the above (3°) of the system. The well-posedness of the system is shown for the symmetric hyperbolic system if the characteristic matrix is independent of  $u$ , while if it depends on  $u$  we know only the limited proof for the well-posedness. From the mathematical point of view, to prove well-posedness with less strict conditions is one of the old but ongoing research problems.

We can define another hyperbolic system between the weakly and symmetric levels. For example, we say strongly hyperbolic (or diagonalizable hyperbolic [19]) system, if the characteristic matrix is diagonalizable and has all real eigenvalues. These inclusion relation is, then,

$$\text{symmetric hyperbolic} \in \text{strongly hyperbolic} \in \text{weakly hyperbolic}. \quad (2.2)$$

We do not repeat each level's features here (see §2 of [19]). However, at the strongly hyperbolic level, we can prove the finiteness of the energy norm if the characteristic matrix is independent of  $u$  (cf [16]), that is one step definitely advanced than a weakly hyperbolic form.

From the point of numerical applications, to write down the fundamental equation in an explicit hyperbolic form gives us great advantages. This is not only from its mathematical well-posed features. It is well known that a certain flux conservative hyperbolic systems of equations is taken as an essential formulation in the computational Newtonian hydrodynamics [28]. Or by using the characteristic speed (eigenvalues) of the system, we can implement the boundary condition [29].

## B. Hyperbolic formulations of the Einstein equation

As was discussed by Geroch [30], most physical systems can be expressed as symmetric hyperbolic systems. However, the standard ADM system does not form a first order hyperbolic system. This can be seen immediately from the fact that the ADM dynamical equations

$$\partial_t \gamma_{ij} = -2NK_{ij} + \nabla_j N_i + \nabla_i N_j, \quad (2.3)$$

$$\begin{aligned} \partial_t K_{ij} = & N( {}^{(3)}R_{ij} + \text{tr}K K_{ij}) - 2NK_{im}K_j^m - \nabla_i \nabla_j N \\ & + (\nabla_j N^m)K_{mi} + (\nabla_i N^m)K_{mj} + N^m \nabla_m K_{ij}, \end{aligned} \quad (2.4)$$

have Ricci curvature  ${}^{(3)}R_{ij}$  which includes the inverse of the 3-metric  $\gamma_{ij}$  by definition. (The notation here is the standard one.  $K_{ij}$  is the extrinsic curvature,  $N$  and  $N^i$  are the lapse and shift vector, respectively.  $\nabla$  denotes a covariant derivative on three-surface.) For our later convenience, we also write down the ADM constraint equations,

$$\mathcal{C}_H^{\text{ADM}} := {}^{(3)}R + (\text{tr}K)^2 - K_{ij}K^{ij} \approx 0, \quad (2.5)$$

$$\mathcal{C}_M^{\text{ADM}i} := \nabla_j (K^{ij} - \gamma^{ij} \text{tr}K) \approx 0, \quad (2.6)$$

which are called the Hamiltonian and momentum constraint equation, respectively.

So far, several first order hyperbolic systems of the Einstein equation have been proposed; some of them are flux conservative [9,10], some of them are symmetrizable (strongly hyperbolic) or symmetric hyperbolic systems [12,14,31,32]. There are many variations in the methods to construct higher hyperbolic systems, but commonly the number of the fundamental dynamical variables results in larger than that of ADM. Several numerical tests are reported (as we referred in the Introduction) using a particular hyperbolic formulation, but no numerical comparisons between these formulations are reported [33].

Using Ashtekar's formulation, we can compare three levels of hyperbolicity in the same interface (same fundamental variables) as we describe next.

## C. Hyperbolic formulations in the Ashtekar formulations

We display here our fundamental dynamical equations. Our notations and more detail review are presented in the Appendix A, but we repeat them here if necessary.

The basic new variables are the densitized inverse triad,  $\tilde{E}_a^i$ , and SO(3,C) self-dual connection,  $\mathcal{A}_i^a$ , where the indices  $i, j, \dots$  indicates the 3-spacetime, and  $a, b, \dots$  is for SO(3) space. The total four-dimensional spacetime is described together with the gauge variables  $\tilde{N}, N^i, \mathcal{A}_0^a$ , which we call the densitized lapse function, shift vector and the triad lapse function. The system has three constraint equations,

$$\mathcal{C}_H^{\text{ASH}} := (i/2)\epsilon^{ab}{}_c \tilde{E}_a^i \tilde{E}_b^j F_{ij}^c \approx 0, \quad (2.7)$$

$$\mathcal{C}_{Mi}^{\text{ASH}} := -F_{ij}^a \tilde{E}_a^j \approx 0, \quad (2.8)$$

$$\mathcal{C}_{Ga}^{\text{ASH}} := \mathcal{D}_i \tilde{E}_a^i \approx 0, \quad (2.9)$$

which are called the Hamiltonian, momentum, and Gauss constraint equation, respectively. The dynamical equations for a set of  $(\tilde{E}_a^i, \mathcal{A}_i^a)$  are

$$\partial_t \tilde{E}_a^i = -i\mathcal{D}_j(\epsilon^{cb} \tilde{N} \tilde{E}_c^j \tilde{E}_b^i) + 2\mathcal{D}_j(N^{lj} \tilde{E}_a^i) + i\mathcal{A}_0^b \epsilon_{ab}{}^c \tilde{E}_c^i, \quad (2.10)$$

$$\partial_t \mathcal{A}_i^a = -i\epsilon^{ab}{}^c \tilde{N} \tilde{E}_b^j F_{ij}^c + N^j F_{ji}^a + \mathcal{D}_i \mathcal{A}_0^a, \quad (2.11)$$

where  $F_{ij}^a := 2\partial_{[i}\mathcal{A}_{j]}^a - i\epsilon^a{}_{bc}\mathcal{A}_i^b\mathcal{A}_j^c$  is the curvature 2-form.

We have to consider the reality conditions when we treat this formalism to describe the classical Lorentzian spacetime. As we review in §A 2, the metric will remain on its real-valued constraint surface during time evolution automatically if we prepare the initial data as it satisfies the reality condition. More practically, we further impose our triad is real-valued. But again this reality condition appears as a gauge restriction on  $\mathcal{A}_0^a$ , (A11), which can be imposed at every time steps. In our actual simulation, we prepare our initial data using the standard ADM approach, so that we have no difficulties to keep these reality conditions.

The set of dynamical equations (2.10) and (2.11) [hereafter we call these the *original equations*] does present a weakly hyperbolic form [19], so that we regard that the mathematical structure of the original equations is one step advanced than ADM. Further, we can construct more higher level of hyperbolic systems by restricting the gauge condition and/or by adding constraint terms,  $\mathcal{C}_H^{\text{ASH}}, \mathcal{C}_{M_i}^{\text{ASH}}$  and  $\mathcal{C}_{G_a}^{\text{ASH}}$ , to the original equations [19]. We extract only the final expressions here.

In order to obtain a symmetric hyperbolic system <sup>2</sup>, we add constraint terms to (2.10) and (2.11) as:

$$\begin{aligned} \text{adding term for } \partial_t \tilde{E}_a^i &= P^i{}_{ab} \mathcal{C}_G^{\text{ASH}b} \\ &\equiv (N^i \delta_{ab} + i\tilde{N} \epsilon_{ab}{}^c \tilde{E}_c^i) \mathcal{C}_G^{\text{ASH}b}, \end{aligned} \quad (2.12)$$

$$\begin{aligned} \text{adding term for } \partial_t \mathcal{A}_i^a &= Q_i^a \mathcal{C}_H^{\text{ASH}} + R_i{}^{ja} \mathcal{C}_{M_j}^{\text{ASH}} \\ &\equiv (e^{-2} \tilde{N} \tilde{E}_i^a) \mathcal{C}_H^{\text{ASH}} + (ie^{-2} \tilde{N} \epsilon^{ac}{}_{b} \tilde{E}_i^b \tilde{E}_c^j) \mathcal{C}_{M_j}^{\text{ASH}}, \end{aligned} \quad (2.13)$$

and also require the gauge condition

$$\mathcal{A}_0^a = \mathcal{A}_i^a N^i, \quad \partial_i N = 0. \quad (2.14)$$

We remark here that this system is obtained within the triad reality condition, and that all adjusted coefficients,  $P^i{}_{ab}, Q_i^a, R_i{}^{ja}$  are uniquely determined.

We can also construct a strongly (or diagonalizable) hyperbolic system by restricting a gauge  $N^l \neq 0, \pm N \sqrt{\gamma^{ll}}$  (where  $\gamma^{ll}$  is the three-metric and we do not take sum here) for the original equations (2.10), (2.11). Or we can also construct from adjusted equations, (2.10)+(2.12) and (2.11)+(2.13) together with the gauge condition

$$\mathcal{A}_0^a = \mathcal{A}_i^a N^i. \quad (2.15)$$

As for the strongly hyperbolic system, we hereafter take the latter expression.

### III. NUMERICAL METHOD

#### A. Overview

We coded up the program so as to compare the evolutions of spacetime with different set of dynamical equations but with the common conditions: the same initial data, the same boundary conditions, the same slicing condition and the same evolution scheme.

We consider the plane symmetric vacuum spacetime without cosmological constant. This spacetime has the true freedom of gravitational wave of two polarized (+ and ×) modes. We apply the periodic boundary conditions to remove any difficulties caused by boundary treatment. The initial data are given by solving constraint equations in ADM variables, using the standard conformal approach by York and O’Murchadha [35]. When we use Ashtekar’s variables for evolution, we transform ADM initial data to Ashtekar’s. The results are analyzed by monitoring the violation of constraint equations which are again compared expressed using the same (or transformed if necessary) variables.

We describe our procedures in the following subsections in detail.

---

<sup>2</sup>As for a symmetric hyperbolic expression, Iriondo et al [34] presented in a different form. The differences between ours and theirs are discussed in [19,20]

## B. metric and the initial value construction

We consider the plane symmetric metric,

$$ds^2 = (-N^2 + N_x N^x) dt^2 + 2N_x dx dt + \gamma_{xx} dx^2 + \gamma_{yy} dy^2 + \gamma_{zz} dz^2 + 2\gamma_{yz} dy dz \quad (3.1)$$

where the components are the function of  $N(x, t)$ ,  $N_x(x, t)$ ,  $\gamma_{xx}(x, t)$ ,  $\gamma_{yy}(x, t)$ ,  $\gamma_{zz}(x, t)$ ,  $\gamma_{yz}(x, t)$ .  $N$  and  $N^x$  are called the lapse function and the shift vector.

We prepare our initial data by solving ADM constraint equations, (2.5) and (2.6), using conformal approach [35]. Since we consider only the vacuum spacetime, the input quantities are the initial guess of the 3-metric,  $\hat{\gamma}_{ij}$ , trace part of the extrinsic curvature,  $\text{tr}K$ , and the transverse traceless part of the extrinsic curvature  $\hat{A}_{TT}$ . For simplicity, we impose  $\hat{A}_{TT} = 0$  and  $\text{tr}K = K_0(\text{const.})$ . The Hamiltonian constraint, then, becomes an equation for the conformal factor,  $\psi$ ,

$$8\hat{\Delta}\psi := 8\frac{1}{\sqrt{\hat{\gamma}}}\partial_i(\hat{\gamma}^{ij}\sqrt{\hat{\gamma}}\partial_j\psi) = \hat{R}\psi + \frac{2}{3}(K_0)^2\psi^5, \quad (3.2)$$

where  $\hat{\gamma} = \det \hat{\gamma}_{ij}$ . The momentum constraint is automatically satisfied in our assumption. The initial dynamical quantities  $\gamma_{ij}$ ,  $K_{ij}$  are given by the conformal transformation,

$$\gamma_{ij} = \psi^4 \hat{\gamma}_{ij}, \quad K_{ij} = \frac{1}{3}\psi^4 \hat{\gamma}_{ij} K_0. \quad (3.3)$$

We solve (3.2) under the periodic boundary condition using the incomplete Cholesky conjugate gradient (ICCG) method.

We have better remark the fact here that we have to assume non-zero  $K_0$  for a model of gravitational pulse waves under the periodic boundary condition in this plane symmetric spacetime. This is shown as follows. Suppose we set  $K_0 = 0$ . From (3.2), we get

$$\partial_x \psi = \frac{1}{\sqrt{\hat{\gamma}}g^{xx}} \int \sqrt{\hat{\gamma}} R \psi dx. \quad (3.4)$$

If we set the boundary as  $x = [A, B]$ , eq. (3.4) becomes

$$\partial_x \psi|_{x=A} - \partial_x \psi|_{x=B} = \frac{1}{\sqrt{\hat{\gamma}}g^{xx}} \int_B^A \sqrt{\hat{\gamma}} R \psi dx. \quad (3.5)$$

However this is inconsistent with the periodic boundary condition, which gives  $\partial_x \psi|_{x=A} = \partial_x \psi|_{x=B}$ , when there exist a gravitational wave pulse which produces  $R \neq 0$  in the region. Therefore we need to assume non-zero  $K_0$  in order to compensate the curvature which is produced by the pulse waves.

Actually such a trace of the extrinsic curvature appears only in the quadratic form. So that we can interpret that our (background) spacetime is either expanding,  $K_0 < 0$ , or contracting,  $K_0 > 0$ . However, this fact indicates that there is no known exact solution to compare with. If the spacetime is allowed to be flat background ( $K_0 = 0$ ), then we know there is a series of exact solutions which describes a collision of plane gravitational waves which were originally found by Szekeres and Khan-Penrose [36]. The formation of curvature singularity after such colliding waves is known to be generic, but that is not generalized for the expanding background (as discussed using numerical simulations [37,38]).

We can set two different modes of gravitational waves. One is the  $+$ -mode waves, which is given by setting a conformal guess metric as (in a matrix form)

$$\hat{\gamma}_{ij} = \begin{pmatrix} 1 & 0 & 0 \\ 1 + a \exp(-b(x-c)^2) & 0 & 0 \\ 1 - a \exp(-b(x-c)^2) & 0 & 0 \end{pmatrix} \quad (3.6)$$

where  $a, b, c$  are parameters. The other is the  $\times$ -mode waves, given by

$$\hat{\gamma}_{ij} = \begin{pmatrix} 1 & 0 & 0 \\ 1 & a \exp(-b(x-c)^2) & 0 \\ 0 & 0 & 1 \end{pmatrix} \quad (3.7)$$

where  $a, b, c$  are parameters again. Both cases, we expect non-linear behavior when wave's curvature becomes quite large compared to the background. In the collision of  $+$ -mode wave and  $\times$ -mode wave, we can also expect to see mode-mixing phenomena which is known as gravitational Faraday effect. These effects are confirmed in our numerical simulations.

### C. Transformation: From ADM to Ashtekar

We need to transform the dynamical variables once on the initial data when we evolve them in the connection variables. We list the procedures to obtain  $(\tilde{E}_a^i, \mathcal{A}_i^a)$  from  $(\gamma_{ij}, K_{ij})$ . These procedures are used also when we evaluate the constraints,  $\mathcal{C}_H^{\text{ASH}}, \mathcal{C}_{Mi}^{\text{ASH}}, \mathcal{C}_{Ga}^{\text{ASH}}$  for the data evolved using ADM variables.

From three-metric  $\gamma_{ij}$  to  $\tilde{E}_a^i$ :

1. Define the correspondent triad  $E_i^a$  to three-metric  $\gamma_{ij}$ . We set

$$E_i^a = \begin{bmatrix} E_x^1 & E_y^1 & E_z^1 \\ E_x^2 & E_y^2 & E_z^2 \\ E_x^3 & E_y^3 & E_z^3 \end{bmatrix} = \begin{bmatrix} \sqrt{\gamma_{xx}} & 0 & 0 \\ 0 & b & d \\ 0 & e & c \end{bmatrix}. \quad (3.8)$$

We set simply  $d = e$ . The relation between the metric and the triad becomes

$$b^2 + d^2 = \gamma_{yy}, \quad c^2 + d^2 = \gamma_{zz}, \quad (b+c)d = \gamma_{yz}. \quad (3.9)$$

For the case of +-mode waves, we define naturally,  $b = \sqrt{\gamma_{yy}}, c = \sqrt{\gamma_{zz}}, d = 0$ . For  $\times$ -mode waves, we also take a natural set of definitions,  $b = [(\gamma_{yy} + (\gamma_{yy}^2 - \gamma_{yz}^2)^{1/2})/2]^{1/2}$  and  $d = \gamma_{yz}/2b$  which are given by solving  $b^2 + d^2 = \gamma_{yy}$  and  $2bd = \gamma_{yz}$ .

2. prepare the inverse triad  $E_a^i$  from triad  $E_i^a$ .
3. calculate the density,  $e$ , as  $e = \det E_i^a$ .
4.  $\tilde{E}_a^i = eE_a^i$ .

From three-metric  $(\gamma_{ij}, K_{ij})$  to  $\mathcal{A}_i^a$ :

1. prepare the triad  $E_i^a$  and its inverse  $E_a^i$ .
2. calculate the connection 1-form  $\omega_i^{bc} = E^{b\mu} \nabla_i E_\mu^c$ . This is expressed only using partial derivatives as <sup>3</sup>

$$\omega_i^{bc} = E^{jb} \partial_{[i} E_{j]}^c - E_{id} E^{kb} E^{jc} \partial_{[k} E_{j]}^d + E^{jc} \partial_{[j} E_{i]}^b. \quad (3.10)$$

3.  $\mathcal{A}_i^a = -K_{ij} E^{ja} - \frac{i}{2} \epsilon^a{}_{bc} \omega_i^{bc}$ .

### D. Transformation: From Ashtekar to ADM

Contrary to the previous transformation, we also need to express  $(\gamma_{ij}, K_{ij})$  from  $(\tilde{E}_a^i, \mathcal{A}_i^a)$  when we evaluate the metric output or ADM constraints when we evolve the spacetime using connection variables. This process is only required at the time of evaluations, and is not required at every time steps unless we use the gauge condition which is primary defined using ADM quantities.

From densitized inverse triad  $\tilde{E}_a^i$  to three-metric  $\gamma_{ij}$ :

1. calculate the density  $e$  as  $e = (\det \tilde{E}_a^i)^{1/2}$ .
2. get the three inverse metric as  $\gamma^{ij} = \tilde{E}_a^i \tilde{E}_a^j / e^2$ .
3. obtain  $\gamma_{ij}$ .

---

<sup>3</sup>This is from the definitions,  $\omega_i^{bc} := E^{jb} \nabla_i E_j^c$  and  $\omega^{abc} := E^{ja} \omega_j^{bc}$ , and a relation

$$3\omega^{[abc]} - 2\omega^{[bc]a} = \omega^{a[bc]} + \omega^{b[ca]} + \omega^{c[ab]} - \omega^{abc} + \omega^{cba} = \omega^{abc}.$$

From  $(\tilde{E}_a^i, \mathcal{A}_i^a)$  to the extrinsic curvature  $K_{ij}$ :

1. prepare the un-densitized inverse triad,  $E_a^i = \tilde{E}_a^i/e$ .
2. prepare triad  $E_i^a$ .
3. calculate the connection 1-form  $\epsilon^a{}_{bc}\omega_i^{bc}$ .
4. calculate  $Z_i^a$ , which is defined as <sup>4</sup>  $Z_i^a := -\mathcal{A}_i^a + \frac{i}{2}\epsilon^a{}_{bc}\omega_i^{bc}(= K_{ij}E^{ja})$ , and get  $K_{ij} = Z_i^a E_{ja}$ .

### E. Evolution equations

We evolve the initial data with different evolution equations and compare its stability. In Table.I, we summarized the equations to be used.

system	variables	Eqs of motion	remark
ADM	$(\gamma_{ij}, K_{ij})$	(2.3), (2.4)	
I Ashtekar (weakly hyp.)	$(\tilde{E}_a^i, \mathcal{A}_i^a)$	(2.10), (2.11) (original)	
II Ashtekar (strongly hyp.)	$(\tilde{E}_a^i, \mathcal{A}_i^a)$	(2.10)+(2.12), (2.11)+(2.13)	(2.15)
III Ashtekar (symmetric hyp.)	$(\tilde{E}_a^i, \mathcal{A}_i^a)$	(2.10)+(2.12), (2.11)+(2.13)	(2.14)

TABLE I. List of systems that we compare.

We here remark again for our slicing (gauge) condition. As for the primary tests, we apply (1) the simplest geodesic slicing condition for the lapse function, (2) simplest zero shift vector  $N^x = 0$ , and (3) natural choice of triad lapse function  $\mathcal{A}_0^a = \mathcal{A}_i^a N^i [= 0$  if  $N^x = 0$ , which is suggested from (2.14) or (2.15)]. However, in the Ashtekar formalism, the densitized lapse function  $\tilde{N}$  is the fundamental gauge quantity rather than  $N$ . Therefore we try two conditions for the lapse, (1a) ADM geodesic slicing condition  $N = 1$ , which will be transformed as  $\tilde{N} = 1/e$  when we evolve in Ashtekar's equations and (1b) Ashtekar geodesic slicing condition  $\tilde{N} = 1$ , which will be transformed as  $N = e$  when we evolve in ADM equations. (We rescaled the transformed lapse [ $\tilde{N}$  in (1a),  $N$  in (1b)] so as to it has the maximum value as unity, in order to keep our Courant condition.) If we apply ADM geodesic slice, then we can compare the weakly hyperbolic system with symmetric hyperbolic one. Similarly if we apply Ashtekar geodesic slice, then we can compare (original) weakly hyperbolic system with strongly hyperbolic one.

We apply Brailovskaya integration scheme (a second order predictor-corrector method) [39] for the time evolution. This scheme can be expressed schematically as follows. Suppose we have a dynamical equation in a form

$$\partial_t u(x, t) = f(u(x, t), \partial_x u(x, t)). \quad (3.11)$$

Then the scheme for updating  $u$  at a point  $x$  from  $t$  to  $t + \Delta t$  consists from two steps. (1) the predictor step: use data on  $t = t$  for right-hand-side and update  $u(x, t)$  for  $\Delta t$  step as  $\tilde{u}(x, t + \Delta t)$ ,

$$\frac{\tilde{u}(x, t + \Delta t) - u(x, t)}{\Delta t} = f(u(x, t), \partial_x u(x, t)). \quad (3.12)$$

(2) the corrector step: prepare right-hand-side using the updated  $\tilde{u}(x, t + \Delta t)$ , and again update  $u(x, t)$  for  $\Delta t$  step as

$$\frac{u(x, t + \Delta t) - u(x, t)}{\Delta t} = f(\tilde{u}(x, t + \Delta t), \partial_x \tilde{u}(x, t + \Delta t)). \quad (3.13)$$

Note that all derivatives in right-hand-side are assumed to take a center space difference.

This is a quite simple scheme, but gives us reasonably accurate and stable evolutions for our problems. We compared this scheme with so-called iterative Crank-Nicholson scheme (cf. [40]), and confirmed that both gives us the same evolutions but Brailovskaya method requires less computational time.

<sup>4</sup> This is from the original definition of  $\mathcal{A}_i^a$ ,  $\mathcal{A}_i^a := \omega_i^{0a} - (i/2)\epsilon^a{}_{bc}\omega_i^{bc}$ .

## F. Check the constraints

We compare the violation of constraint equations during the time evolution. We have ADM constraint equations,  $\mathcal{C}_H^{\text{ADM}}$  and  $\mathcal{C}_{Mi}^{\text{ADM}}$  [(2.5) and (2.6)], and also Ashtekar's constraint equations,  $\mathcal{C}_H^{\text{ASH}}$ ,  $\mathcal{C}_{Mi}^{\text{ASH}}$  and  $\mathcal{C}_{Ga}^{\text{ASH}}$  [(2.7), (2.8) and (2.9), respectively]. By the transformations between  $(\gamma_{ij}, K_{ij})$  and  $(\tilde{E}_a^i, \mathcal{A}_i^a)$ , we can compare all constraints whatever the evolution system is.

We evaluate the violation of the constraints by (i) its maximum,  $\max_x |\mathcal{C}(x)|$ , (ii) L1 norm,  $(\sum_{x=1}^n \mathcal{C}(x))/n$ , and (iii) L2 norm,  $(\sum_{x=1}^n |\mathcal{C}(x)|^2/n)^{1/2}$ , where  $n$  is the number of the grid points.

The numerical code passed convergence tests, and the results shown in this article are all obtained with acceptable accuracy. In Fig.1, we show a result of a convergence test. The figure shows L2 norm of  $\mathcal{C}_H^{\text{ASH}}$  for the evolution of  $+$ -mode single pulse wave using the original set of Ashtekar's equation. We can see clearly that L2 norm of the error of  $\mathcal{C}_H^{\text{ASH}}$  will decrease in finer resolution cases. (The model is described in the next section.)

All the results we show in this article is obtained using the grid points of 401 for the range  $x = [-5, +5]$ , That is gravitational waves travel all the numerical region with time 10 if the background expansion  $K_0$  is close to zero. We use the Courant number  $\nu = \Delta t/\Delta x$  as 0.2.

We coded up as our all fundamental quantities (metric, gauge variables,  $\dots$ ) are complex, but we observed also that the evolution from our initial data will never break its metric reality conditions. Due to the gauge condition for  $\mathcal{A}_0^a$ , (A11), we also confirmed that our evolutions preserve the triad reality condition.

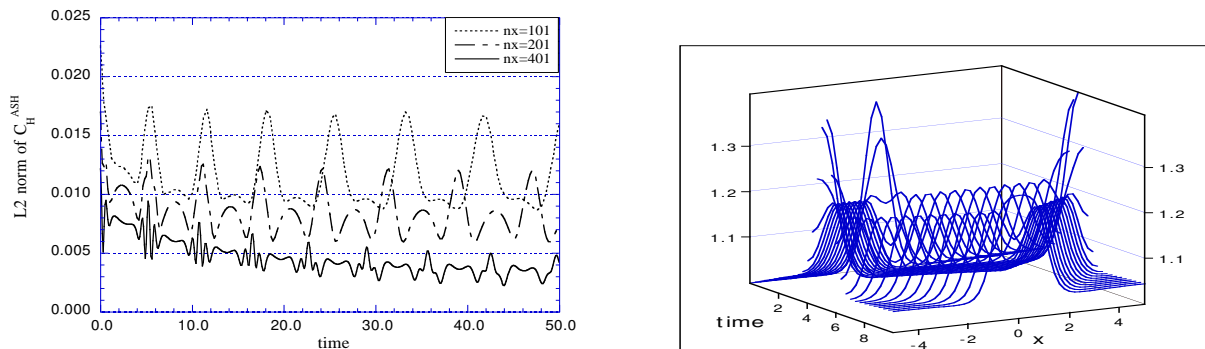


FIG. 1. (a) An example of the convergence tests. L2 norms of  $\mathcal{C}_H^{\text{ASH}}$  for the evolution of  $+$ -mode single pulse wave using the original set of Ashtekar's equation are shown for three resolutions of grid points of 101, 201 and 401 for the range of  $x = [-5, +5]$ . The initial data is a single  $+$ -mode pulse wave with large amplitude [ $a = 0.3, b = 2.0, c = 0.0$  in eq.(3.6)] in the expanding background ( $K_0 = -0.025$ ), and the original Ashtekar's evolution equation with  $\tilde{N} = 1$  lapse condition was used. We can see clearly that the error norm  $\mathcal{C}_H^{\text{ASH}}$  will decrease in finer resolution cases. (b) An image of gravitational wave propagation. The metric component  $g_{yy}$  is plotted for the single initial pulse case which was used for the convergence test in Fig.(a). Only upto time  $t = 10$  is drawn.

## IV. EXPERIMENTS 1: DIFFERENCES BETWEEN HYPERBOLICITIES

In this section, we examine the stability of the numerical evolutions comparing the different hyperbolic systems. We begin showing how the evolutions by Ashtekar's equations are look like comparing with those by ADM equations.

## A. ADM vs Ashtekar

We start describing our model, plane wave propagation in expanding/collapsing spacetime. We prepare the initial data as there exist one or two gravitational pulse waves in our numerical region. The pulse then start propagating in both  $\pm x$  direction with the light speed, and appear from the other side of the numerical region if it pass the boundary, since we apply the periodic boundary condition. When pulses are collide, then the amplitude seems to be just a double as they superposed, but they travel each other in its own original propagation direction. So that we observe something like a solitonic wave pulse propagation.

As we mentioned in §III B, we have to assume our background not to be flat, therefore there is no related exact solutions. The reader might think that if we set  $|\text{tr } K|$  to be small and pulse wave shapes to be quite sharp then our simulations are close to the analytic colliding plane wave solutions which produce the curvature singularity. However, from the numerical stands, these two requirements are opposite (e.g. sharp wave input produces large curvature which should be compensated by  $|\text{tr } K|$  in order to construct our initial data). So that it is not so surprising that our wave propagation behaves like solitons after their collisions.

In Fig.1 (b), we plot an image of wave propagation (metric component  $g_{yy}$ ) upto  $t = 10$ , of the initial data of +-mode one pulse wave located at  $x = 0$ . This model was used for the convergence test [shown as Fig.1 (a)], and it turns out that the system can follow its evolution in proper manner even after the long time integration.

If we switched our evolution system from ADM to Ashtekar's, the fundamental metric output should be quite similar. (These are not necessary completely equivalent, because we need to rescale the lapse function differently, even if we apply the same "condition"  $\partial_x \tilde{N} = \text{const.}$  or  $\partial_x N = \text{const.}$  ) We remark here that Fig.1 was already obtained using Ashtekar's evolution equations. In Fig.2 (a1) and (a2), we plot metric comparison between ADM and Ashtekar's (original/weakly hyperbolic) equations. The initial data for this figure was taken to be two +-mode initial pulses for expanding background spacetime. We see three metric output shows quite similar evolutions. We also plotted a sample of evolution of the fundamental dynamical quantities  $\tilde{E}_2^y$  and  $\mathcal{A}_y^2$  in Fig.2 (b1) and (b2).

We next compare constraint violations by Ashtekar's equation with that of ADM. In Fig.3, we plot the L2 norm of  $\mathcal{C}_H^{\text{ASH}}$  and  $\mathcal{C}_H^{\text{ADM}}$ . We see that ADM evolution shows less violation in measuring  $\mathcal{C}_H^{\text{ADM}}$ , and the Ashtekar evolution shows less violation in measuring  $\mathcal{C}_H^{\text{ASH}}$ . This is, we think, within the numerical truncation error in the process of numerical transformation of variables (ADM to Ashtekar/ Ashtekar to ADM), since they show at the same order of violation, and always better within its formulation. Therefore, it is not appropriate to conclude here which formulation is better than the other.

As the reader guesses, the violations of constraints reduce themselves if the background spacetime is expanding ( $K_0 < 0$ ). Therefore we will use the collapsing background spacetime ( $K_0 > 0$ ) hereafter for presentations, with the expectation of having more non-linear effects, but this direction also stops the time evolution at the finite time.

## B. Comparison between hyperbolicities

We show our comparison of the stability between the different hyperbolicities.

We first compare the (original) weakly hyperbolic system [system I in Table.I] with the strongly hyperbolic system [system II in Table.I]. This comparison can be done under Ashtekar's geodesic slicing condition,  $\tilde{N} = 1$ . We prepare two initial gravitational pulses (both  $+-$  or  $\times - \times$  modes) and set our background is collapsing. In Fig.4, we show the constraint errors,  $\mathcal{C}_H^{\text{ASH}}$  and  $\mathcal{C}_M^{\text{ASH}}$ . We see that strongly hyperbolic system slightly improves the violation of the constraints.

We next compare the (original) weakly hyperbolic system [system I in Table.I] with the symmetric hyperbolic system [system III in Table.I]. This comparison can be done under ADM geodesic slicing condition,  $N = 1$ . We repeat the same experiments as above and showed plots in Fig.5. We again see that symmetric hyperbolic system slightly improves the situation.

From both Figs. 4 and 5, we see that strongly and symmetric hyperbolic system produce less violation of constraints than the original weakly hyperbolic system. Therefore one conclusion is that adjusting the equation of motion with constraint terms, (2.12) and (2.13), does definitely make the system stable. However the difference is not so drastic to change the orders of magnitude of its violation of constraints.

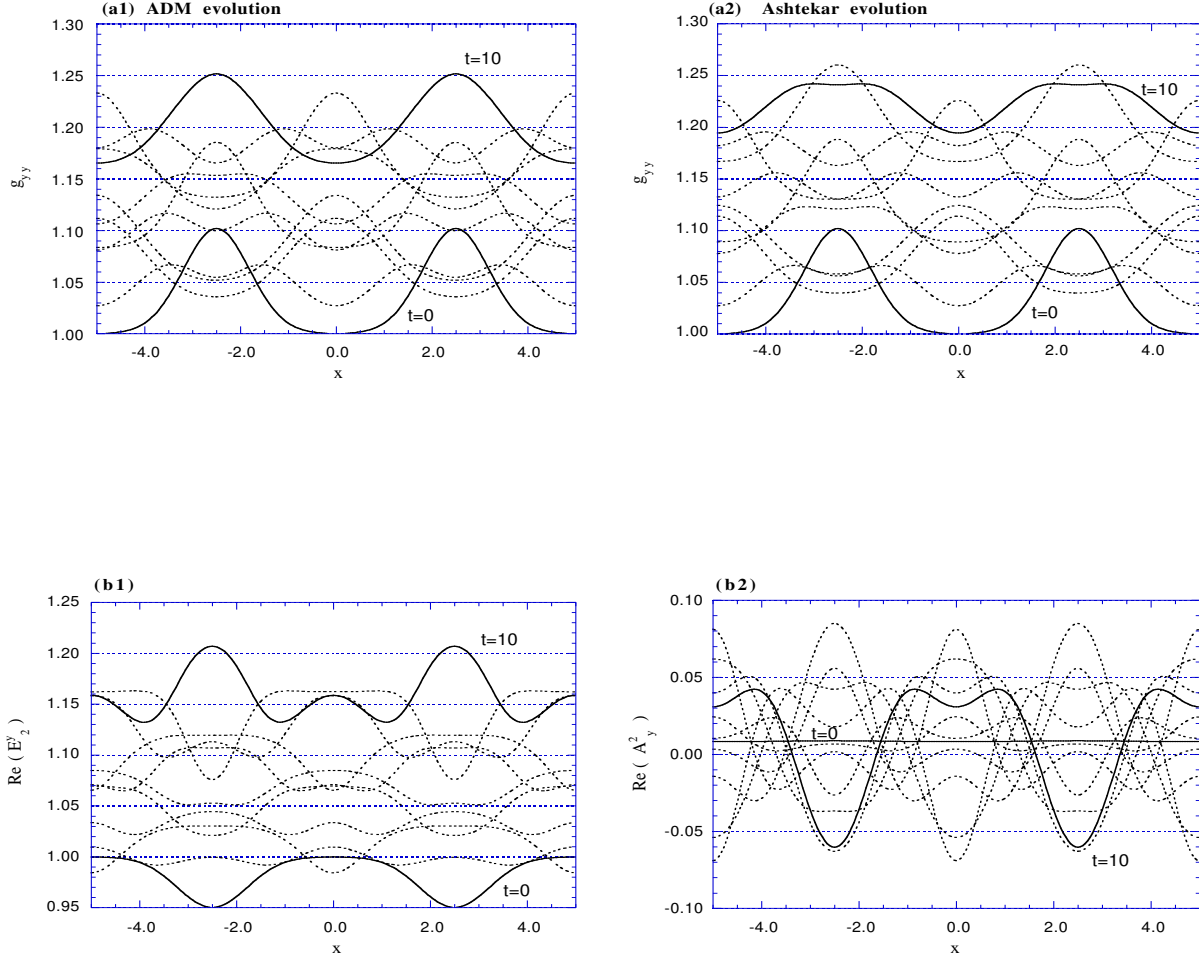


FIG. 2. A comparison of evolution by Ashtekar's equation with that of ADM. The same initial data of two  $+$ -mode pulse waves, and the same slicing condition,  $\tilde{N} = 1$  is applied. Figs. (a1) and (a2) are of three-metric component  $g_{yy}$ , at the snapshot of  $t = 0, 1, \dots, 10$ . Figs. (b1) and (b2) are of the densitized triad  $\tilde{E}_2^y$ , and the connection  $\mathcal{A}_y^2$ , respectively, for the case of Ashtekar evolution was used.

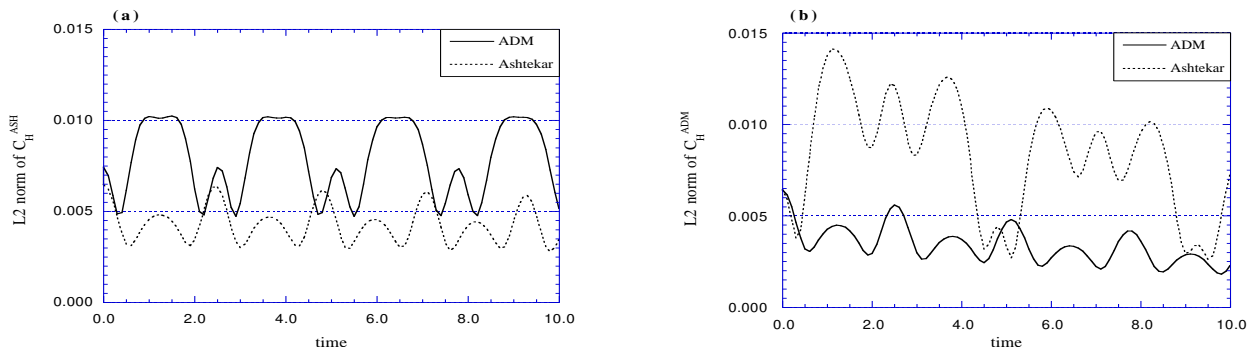


FIG. 3. Comparison of constraint violations by Ashtekar's equation with that of ADM. (a) L2 norm of Ashtekar's Hamiltonian constraint equation,  $\mathcal{C}_H^{\text{ASH}}$ . (b) L2 norm of ADM's Hamiltonian constraint equation,  $\mathcal{C}_H^{\text{ADM}}$ . The evolutions of Fig.2 are applied.

## V. EXPERIMENTS 2: ANOTHER WAY TO CONTROL THE STABILITY

The results we presented in the previous section indicate that both strongly and symmetric hyperbolic systems show better performance than the original weakly hyperbolic system. These systems are obtained by adding constraint terms, (2.12) and (2.13), (we say adjusted terms) to right-hand-side of the original equation, (2.10) and (2.11). We, in this section, show our simple experiments of changing the magnitude of the multipliers of such adjusted terms.

We now consider the system, which equations of motion, (2.10) and (2.11), are adjusted as

$$\begin{aligned} \text{adding term for } \partial_t \tilde{E}_a^i &= \kappa P_{ab}^i \mathcal{C}_G^{\text{ASH}b} \\ &\equiv \kappa (N^i \delta_{ab} + i \tilde{N} \epsilon_{ab}{}^c \tilde{E}_c^i) \mathcal{C}_G^{\text{ASH}b}, \end{aligned} \quad (5.1)$$

$$\begin{aligned} \text{adding term for } \partial_t \mathcal{A}_i^a &= \kappa Q_i^a \mathcal{C}_H^{\text{ASH}} + \kappa R_i{}^{ja} \mathcal{C}_{Mj}^{\text{ASH}} \\ &\equiv \kappa (e^{-2} \tilde{N} \tilde{E}_i^a) \mathcal{C}_H^{\text{ASH}} + \kappa (i e^{-2} \tilde{N} \epsilon^{ac}{}_b \tilde{E}_i^b \tilde{E}_c^j) \mathcal{C}_{Mj}^{\text{ASH}}, \end{aligned} \quad (5.2)$$

where we introduce a (real-valued) constant,  $\kappa$ . The set of (2.10)+(5.1) and (2.11)+(5.2) becomes the original weakly hyperbolic system if  $\kappa = 0$  or  $1/2$ , becomes the symmetric hyperbolic system if  $\kappa = 1$  and  $N = \text{const.}$ , and remains strongly hyperbolic systems for other choices of  $\kappa$ . We remark that the coefficients for constructing the symmetric hyperbolic system are uniquely determined and there is no other additional terms (say, no  $\mathcal{C}_H^{\text{ASH}}, \mathcal{C}_M^{\text{ASH}}$  for  $\partial_t \tilde{E}_a^i$ , no  $\mathcal{C}_G^{\text{ASH}}$  for  $\partial_t \mathcal{A}_i^a$ ) [19].

We tried the same evolutions as in the previous section but changing  $\kappa$  in eqs. (5.1) and (5.2). In Fig.6, we plot the L2 norm of the Hamiltonian and momentum constraint equations,  $\mathcal{C}_H^{\text{ASH}}$  and  $\mathcal{C}_M^{\text{ASH}}$ . We see  $\kappa = 0$  and  $1$  produce the same results with those of weakly and symmetric hyperbolic systems, but  $\kappa = 2$  and  $3$  produce better performance than the symmetric hyperbolic system, although these cases are of strongly hyperbolic levels. Therefore, as far as monitoring the violation of the constraints, we may say the symmetric hyperbolic form is not always the best.

We also tried the similar experiments in the vacuum Maxwell equation. We show the details and a figure in the appendix B, but shortly the symmetric hyperbolic system shows the best performance in the Maxwell system (but also strongly hyperbolic system shows the similar performance). We should remark that the original Maxwell equation forms a symmetric hyperbolicity, and additional terms due to  $\kappa$  reduce hyperbolicity to strongly or weakly level.

These experiments of changing  $\kappa$  are now in progress and supposed to be reported in our Paper II [41]. There, we propose a plausible explanation why such adjusted terms work for stabilizing the system. Shortly, we will conjecture the criterion using the eigenvalues of the constraint propagation equations of its 'adjusted version'.

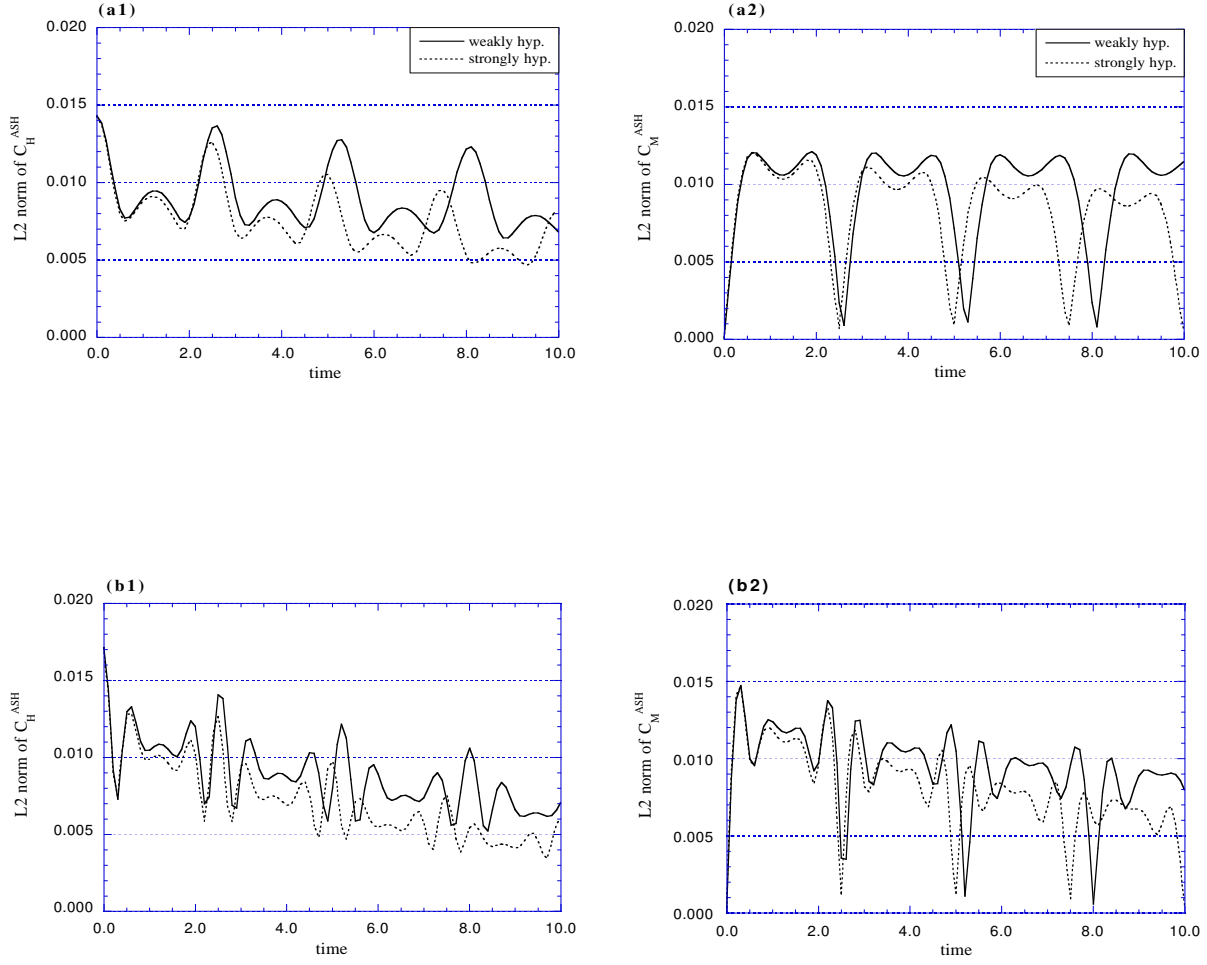


FIG. 4. Comparison of the strongly hyperbolic system with the weakly hyperbolic system ( $\tilde{N} = 1$  slice). For the initial data of  $+$ -mode waves and  $\times$ -mode waves, we plot the constraint violations for the Hamiltonian and momentum constraints. Figs. (a1) and (a2) are of  $+$ -mode waves propagation and L2 norm of  $C_H^{\text{ASH}}$  and  $C_M^{\text{ASH}}$ , respectively. Figs. (b1) and (b2) are of  $\times$ -mode waves propagation and L2 norm of  $C_H^{\text{ASH}}$  and  $C_M^{\text{ASH}}$ , respectively. We see from all of them that strongly hyperbolic system improves the violation of the constraints.

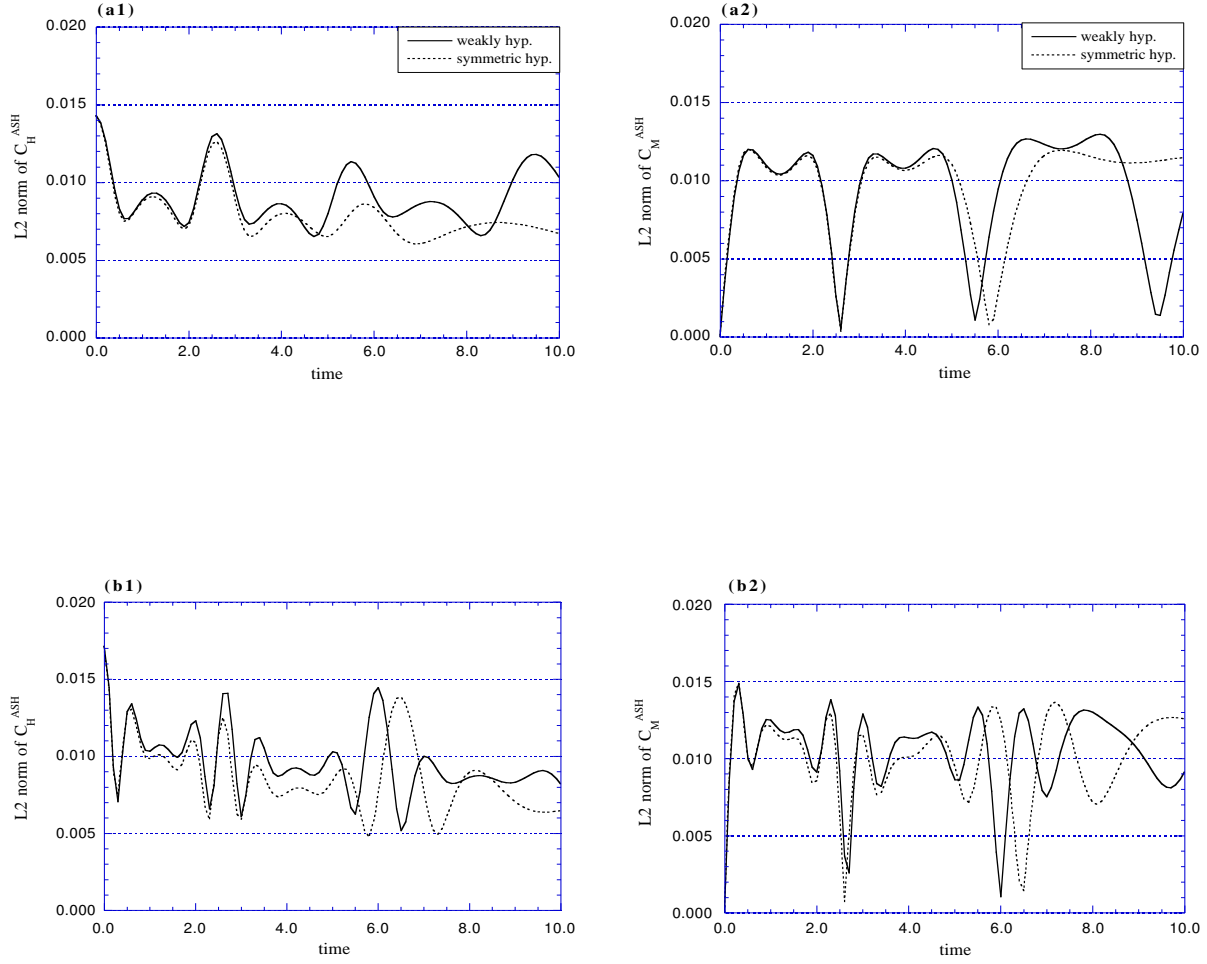


FIG. 5. Comparison of the symmetric hyperbolic system with the weakly hyperbolic system ( $N = 1$  slice), as the same way with Fig.4. Figs. (a1) and (a2) are of  $+$ -mode waves propagation and L2 norm of  $C_H^{ASH}$  and  $C_M^{ASH}$ , respectively. Figs. (b1) and (b2) are of  $\times$ -mode waves propagation and L2 norm of  $C_H^{ASH}$  and  $C_M^{ASH}$ , respectively. We see from all of them that symmetric hyperbolic system improves the violation of the constraints.

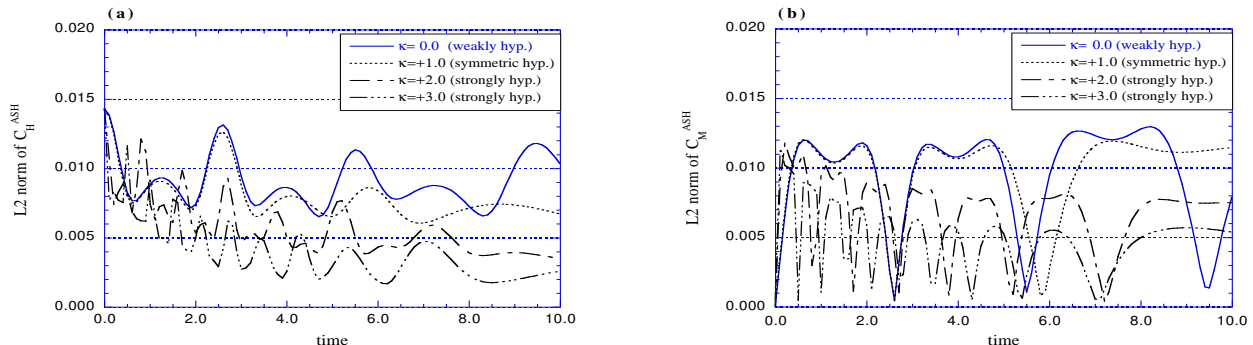


FIG. 6. Comparisons of ‘adjusted’ system with the different multiplier,  $\kappa$ , in eqs. (5.1) and (5.2). Plots are of L2 norm of the Hamiltonian and momentum constraint equations,  $C_H^{ASH}$  and  $C_M^{ASH}$  [Figs.(a) and (b)] respectively. We see some  $\kappa$  produce better performance than the symmetric hyperbolic system.

## VI. DISCUSSION

Motivated by the recent many proposals of the hyperbolic formulations of the Einstein equation, we studied numerically these stability properties with the purpose of comparing three mathematical levels of hyperbolicity: weakly hyperbolic, strongly hyperbolic, and symmetric hyperbolic systems. We apply Ashtekar’s connection formulation, because this is the only known system which we can compare three hyperbolic levels with the same interface.

Our numerical code demonstrates gravitational wave propagation in the plane symmetric spacetime, and we compare the “stability” by monitoring the violation of the constraints. By comparing the results obtained from the weakly hyperbolic system, we observe the strongly and symmetric hyperbolic system show the better stability property, but not so much difference between the latter two. Therefore we may conclude that hyperbolic formulations help the numerics as we expected.

However, we also find that the symmetric hyperbolic system is not always the best for controlling stability, by taking the multiplier for adjusted terms in the equations of motion. This result suggests that a certain kind of hyperbolicity is enough for controlling the violation of constraint equation. In our case it is the strongly hyperbolic level. This statement is also obtained from an experiment in Maxwell system.

Why we can get the better stability by adding constraint terms in the dynamical equations? The added terms are basically *error* terms during the evolution. A plausible explanation we have now is by evaluating the eigenvalues of the the constraint propagation equations (of its adjusted version). Even if we added *error* terms in the equations, the system propagates to a constrained surfaces when its constraint propagation equations suggest the decay of the constraints. This was an essential reason of the so-called  $\lambda$ -system [22,21]. In our succeeding paper [41], we will discuss this point in detail together with a numerical demonstration of  $\lambda$ -systems.

In the end, we are glad to announce that Ashtekar’s connection variables are finally applied in numerical simulations. This new approach, we hope, contributes to understand further gravitational physics, and opens a new window to peel off interesting non-linear features in the future.

## ACKNOWLEDGEMENTS

HS appreciates helpful comments by Abhay Ashtekar, Jorge Pullin, Douglas Arnold, L. Samuel Finn, and Mijan Huq, and the hospitality of the CGPG group. Numerical computations were performed using machines at CGPG. HS was supported by the Japan Society for the Promotion of Science as a research fellow abroad.

† Electronic address: shinkai@gravity.phys.psu.edu

‡ Electronic address: yoneda@mn.waseda.ac.jp

- [1] M.W. Choptuik, Phys. Rev. Lett. **70**, 9 (1993).
- [2] The latest reviews are available in the proceedings of *Black Holes and Gravitational Waves* ed. by T. Nakamura and H. Kodama, as the issue of Prog. Theor. Phys. Suppl. **136** (1999).
- [3] T. Nakamura, K. Oohara and Y. Kojima, Prog. Theor. Phys. Suppl. **90**, 1 (1987). M. Shibata and T. Nakamura, Phys. Rev. **D52**, 5428 (1995).
- [4] T. W. Baumgarte and S. L. Shapiro, Phys. Rev. **D59**, 024007 (1999). T. W. Baumgarte, S.A. Hughes, and S. L. Shapiro, *ibid.* **D60**, 087501 (1999).
- [5] M. Alcubierre, *et al.* gr-qc/0003071.
- [6] M. Alcubierre, *et al.* gr-qc/9908079.
- [7] Recent reviews are given by, *e.g.*, O. A. Reula, Living Rev. Relativ. **1998-3** at <http://www.livingreviews.org/>; H. Friedrich and A. Rendall, in *Einstein's field equations and their physical interpretation*, ed. by B.G.Schmidt (Springer, Berlin 2000), available as gr-qc/0002074.
- [8] S. Frittelli, Phys. Rev. **D55**, 5992 (1997).
- [9] C. Bona, J. Massó, E. Seidel and J. Stela, Phys. Rev. Lett. **75**, 600 (1995); Phys. Rev. **D56**, 3405 (1997).
- [10] C. Bona, J. Massó, Phys. Rev. Lett. **68**, 1097 (1992).
- [11] M.A. Scheel, T.W. Baumgarte, G.B. Cook, S.L. Shapiro, and S.A. Teukolsky, Phys. Rev. **D56** 6320 (1997); *ibid.* **D58**, 044020 (1998).
- [12] Y. Choquet-Bruhat and J.W. York, Jr., C. R. Acad. Sci. Paris, **t. 321**, Série I, 1089 (1995) [gr-qc/9506071]; A. Abrahams, A. Anderson, Y. Choquet-Bruhat and J.W. York, Jr., Phys. Rev. Lett. **75**, 3377 (1995); C. R. Acad. Sci. Paris, **t. 323**, Série II b, 835 (1996); Class. Quantum Grav. **14**, A9 (1997); A. Anderson and J.W. York, Jr. Phys. Rev. Lett. **82**, 4384 (1999).
- [13] M. Alcubierre, Phys. Rev. **D55**, 5981 (1997); M. Alcubierre and J. Massó, Phys. Rev. **D57**, 4511 (1998).
- [14] H. Friedrich, Proc. Roy. Soc. **A375**, 169 (1981); Proc. Roy. Soc. **A378**, 401 (1981); Comm. Math. Phys **100**, 525 (1985); J. Diff. Geom. **34**, 275 (1991); Class. Quantum Grav. **13**, 1451 (1996).
- [15] J. Frauendiener, Phys. Rev. **D58** 064002 (1998). *ibid.* **D58** 064003 (1998), Class. Quant. Grav. **17** 373 (2000); P. Hübner, Class. Quant. Grav. **16** 2145 (1999), *ibid.* **16** 2823 (1999).
- [16] J.M. Stewart, Class. Quant. Grav. **15**, 2865 (1998).
- [17] A. Ashtekar, Phys. Rev. Lett. **57**, 2244 (1986); Phys. Rev. **D36**, 1587 (1987);
- [18] A. Ashtekar, *Lectures on Non-Perturbative Canonical Gravity* (World Scientific, Singapore, 1991).
- [19] G. Yoneda and H. Shinkai, Int. J. Mod. Phys. D **9**, 13 (2000).
- [20] G. Yoneda and H. Shinkai, Phys. Rev. Lett. **82**, 263 (1999).
- [21] H. Shinkai and G. Yoneda, Phys. Rev. **D60**, 101502 (1999).
- [22] O. Brodbeck, S. Frittelli, P. Hübner and O.A. Reula, J. Math. Phys. **40**, 909 (1999).
- [23] A. Ashtekar and J.D. Romano, "Key (3+1)-equations in terms of new variables for numerical relativity", Syracuse University Report (1989).
- [24] D.C. Salisbury, L.C. Shepley, A. Adams, D. Mann, L.Turvan and B. Turner, Class. Quantum Grav. **11**, 2789 (1994).
- [25] R. Capovilla, T. Jacobson, and J. Dell, Phys. Rev. Lett. **63**, 2325 (1989); Class. Quantum Grav. **8**, 59 (1991).
- [26] A. Ashtekar, J.D. Romano and R. S. Tate, Phys. Rev. **D40**, 2572 (1989).
- [27] G. Yoneda and H. Shinkai, Class. Quantum Grav. **13**, 783 (1996).
- [28] *e.g.*, C. Hirsch, *Numerical Computation of Internal and External Flows* vol. I & II, (John Wiley and Sons, 1988)
- [29] C. Bona, J. Massó, E. Seidel and P. Walker, gr-qc/9804052.
- [30] R. Geroch, *Partial Differential Equations in Physics*, gr-qc/9602055.
- [31] A. E. Fischer and J. E. Marsden, Commun. Math. Phys. **28**, 1 (1972).
- [32] S. Frittelli and O.A. Reula, Phys. Rev. Lett. **76**, 4667 (1996).
- [33] Recently, we heard that J. Bardeen and L. Buchman are preparing a numerical comparison between Bona-Massó (97) and Anderson-York (99) formulations.
- [34] M.S. Iriondo, E.O. Leguizamón and O.A. Reula, Phys. Rev. Lett. **79**, 4732 (1997); Adv. Theor. Math. Phys. **2**, 1075 (1998).
- [35] N. O'Murchadha, J.W. York, Jr., Phys. Rev. **D10**, 428 (1974)
- [36] P. Szekeres, Nature **228**, 1183 (1970); J. Math. Phys. **13**, 286 (1972); V.A. Khan and R. Penrose, Nature **229**, 185 (1971).
- [37] J. Centrella and R.A. Matzner, Astrophys. J. **230**, 311 (1979); J. Centrella, Astrophys. J. **241**, 875 (1980); J. Centrella and R.A. Matzner, Phys. Rev. **D25**, 930 (1982).
- [38] H. Shinkai and K. Maeda, Phys. Rev. **D48** 3910 (1993).
- [39] D. Bernstein, D.W. Hobill, and L.L. Smarr, in *Frontiers in Numerical Relativity*, edited by C.R. Evans, L.S. Finn, and D.W. Hobill (Cambridge Univ. Press, 1989)
- [40] S.A. Teukolsky, Phys. Rev. **D61**, 087501 (2000).
- [41] G. Yoneda and H. Shinkai, in preparation. [Paper II]

## APPENDIX A: ASHTEKAR'S FORMULATION OF GENERAL RELATIVITY

We give a brief review of the Ashtekar formulation and the way of handling reality conditions. This appendix is for describing our notations.

### 1. Variables and Equations

The key feature of Ashtekar's formulation of general relativity [17] is the introduction of a self-dual connection as one of the basic dynamical variables. Let us write the metric  $g_{\mu\nu}$  using the tetrad  $E_\mu^I$  as  $g_{\mu\nu} = E_\mu^I E_\nu^J \eta_{IJ}$ <sup>5</sup>. Define its inverse,  $E_I^\mu$ , by  $E_I^\mu := E_\nu^J g^{\mu\nu} \eta_{IJ}$  and we impose  $E_a^0 = 0$  as the gauge condition. We define  $SO(3, \mathbb{C})$  self-dual and anti self-dual connections  ${}^\pm \mathcal{A}_\mu^a := \omega_\mu^{0a} \mp (i/2) \epsilon^a{}_{bc} \omega_\mu^{bc}$ , where  $\omega_\mu^{IJ}$  is a spin connection 1-form (Ricci connection),  $\omega_\mu^{IJ} := E^{I\nu} \nabla_\mu E_\nu^J$ . Ashtekar's plan is to use only the self-dual part of the connection  ${}^+ \mathcal{A}_\mu^a$  and to use its spatial part  ${}^+ \mathcal{A}_i^a$  as a dynamical variable. Hereafter, we simply denote  ${}^+ \mathcal{A}_\mu^a$  as  $\mathcal{A}_\mu^a$ .

The lapse function,  $N$ , and shift vector,  $N^i$ , both of which we treat as real-valued functions, are expressed as  $E_0^\mu = (1/N, -N^i/N)$ . This allows us to think of  $E_0^\mu$  as a normal vector field to  $\Sigma$  spanned by the condition  $t = x^0 = \text{const.}$ , which plays the same role as that of Arnowitt-Deser-Misner (ADM) formulation. Ashtekar treated the set  $(\tilde{E}_a^i, \mathcal{A}_i^a)$  as basic dynamical variables, where  $\tilde{E}_a^i$  is an inverse of the densitized triad defined by  $\tilde{E}_a^i := e E_a^i$ , where  $e := \det E_i^a$  is a density. This pair forms the canonical set.

In the case of pure gravitational spacetime, the Hilbert action takes the form

$$S = \int d^4x [(\partial_t \mathcal{A}_i^a) \tilde{E}_a^i + (i/2) \tilde{N} \tilde{E}_a^i \tilde{E}_b^j F_{ij}^c \epsilon^{ab}{}_c - e^2 \Lambda \tilde{N} - N^i F_{ij}^a \tilde{E}_a^j + \mathcal{A}_0^a \mathcal{D}_i \tilde{E}_a^i], \quad (\text{A1})$$

where  $\tilde{N} := e^{-1} N$ ,  $F_{\mu\nu}^a := 2\partial_{[\mu} \mathcal{A}_{\nu]}^a - i\epsilon^a{}_{bc} \mathcal{A}_\mu^b \mathcal{A}_\nu^c$  is the curvature 2-form,  $\Lambda$  is the cosmological constant,  $\mathcal{D}_i \tilde{E}_a^j := \partial_i \tilde{E}_a^j - i\epsilon_{ab}{}^c \mathcal{A}_i^b \tilde{E}_c^j$ , and  $e^2 = \det \tilde{E}_a^i = (\det E_i^a)^2$  is defined to be  $\det \tilde{E}_a^i = (1/6) \epsilon^{abc} \underline{\epsilon}_{ijk} \tilde{E}_a^i \tilde{E}_b^j \tilde{E}_c^k$ , where  $\epsilon_{ijk} := \epsilon_{abc} E_i^a E_j^b E_k^c$  and  $\underline{\epsilon}_{ijk} := e^{-1} \epsilon_{ijk}$ <sup>6</sup>.

Varying the action with respect to the non-dynamical variables  $\tilde{N}$ ,  $N^i$  and  $\mathcal{A}_0^a$  yields the constraint equations,

$$\mathcal{C}_H^{\text{ASH}} := (i/2) \epsilon^{ab}{}_c \tilde{E}_a^i \tilde{E}_b^j F_{ij}^c - \Lambda \det \tilde{E} \approx 0, \quad (\text{A2})$$

$$\mathcal{C}_{Mi}^{\text{ASH}} := -F_{ij}^a \tilde{E}_a^j \approx 0, \quad (\text{A3})$$

$$\mathcal{C}_{Ga}^{\text{ASH}} := \mathcal{D}_i \tilde{E}_a^i \approx 0. \quad (\text{A4})$$

The equations of motion for the dynamical variables  $(\tilde{E}_a^i$  and  $\mathcal{A}_i^a)$  are

$$\partial_t \tilde{E}_a^i = -i \mathcal{D}_j (\epsilon^{cb}{}_a \tilde{N} \tilde{E}_c^j \tilde{E}_b^i) + 2 \mathcal{D}_j (N^{[j} \tilde{E}_a^{i]}) + i \mathcal{A}_0^b \epsilon_{ab}{}^c \tilde{E}_c^i, \quad (\text{A5})$$

$$\partial_t \mathcal{A}_i^a = -i \epsilon^{ab}{}_c \tilde{N} \tilde{E}_b^j F_{ij}^c + N^j F_{ji}^a + \mathcal{D}_i \mathcal{A}_0^a + \Lambda \tilde{N} \tilde{E}_i^a, \quad (\text{A6})$$

where  $\mathcal{D}_j X_a^{ji} := \partial_j X_a^{ji} - i\epsilon_{ab}{}^c \mathcal{A}_j^b X_c^{ji}$ , for  $X_a^{ij} + X_a^{ji} = 0$ .

### 2. Reality conditions

In order to construct the metric from the variables  $(\tilde{E}_a^i, \mathcal{A}_i^a, \tilde{N}, N^i)$ , we first prepare the tetrad  $E_I^\mu$  as  $E_0^\mu = (1/e\tilde{N}, -N^i/e\tilde{N})$  and  $E_a^\mu = (0, \tilde{E}_a^i/e)$ . Using them, we obtain the metric  $g^{\mu\nu}$  such that  $g^{\mu\nu} := E_I^\mu E_J^\nu \eta^{IJ}$ .

---

<sup>5</sup>We use  $\mu, \nu = 0, \dots, 3$  and  $i, j = 1, \dots, 3$  as spacetime indices, while  $I, J = (0), \dots, (3)$  and  $a, b = (1), \dots, (3)$  are  $SO(1, 3)$ ,  $SO(3)$  indices respectively. We raise and lower  $\mu, \nu, \dots$  by  $g^{\mu\nu}$  and  $g_{\mu\nu}$  (the Lorentzian metric);  $I, J, \dots$  by  $\eta^{IJ} = \text{diag}(-1, 1, 1, 1)$  and  $\eta_{IJ}$ ;  $i, j, \dots$  by  $\gamma^{ij}$  and  $\gamma_{ij}$  (the three-metric);  $a, b, \dots$  by  $\delta^{ab}$  and  $\delta_{ab}$ . We also use volume forms  $\epsilon_{abc} := \epsilon_{abc} \epsilon^{abc} = 3!$ .

<sup>6</sup>When  $(i, j, k) = (1, 2, 3)$ , we have  $\epsilon_{ijk} = e$ ,  $\underline{\epsilon}_{ijk} = 1$ ,  $\epsilon^{ijk} = e^{-1}$ , and  $\tilde{\epsilon}^{ijk} = 1$ .

This metric, in general, is not real-valued in the Ashtekar formulation. To ensure that the metric is real-valued, we need to impose real lapse and shift vectors together with two *metric reality* conditions;

$$\text{Im}(\tilde{E}_a^i \tilde{E}^{ja}) = 0, \quad (\text{A7})$$

$$W^{ij} := \text{Re}(\epsilon^{abc} \tilde{E}_a^k \tilde{E}_b^{(i} \mathcal{D}_k \tilde{E}_c^{j)}) = 0, \quad (\text{A8})$$

where the latter comes from the secondary condition of reality of the metric  $\text{Im}\{\partial_t(\tilde{E}_a^i \tilde{E}^{ja})\} = 0$  [26], and we assume  $\det \tilde{E} > 0$  (see [27]).

For later convenience, we also prepare stronger reality conditions, *triad reality* conditions. The primary and secondary conditions are written respectively as

$$U_a^i := \text{Im}(\tilde{E}_a^i) = 0, \quad (\text{A9})$$

$$\text{and} \quad \text{Im}(\partial_t \tilde{E}_a^i) = 0. \quad (\text{A10})$$

Using the equations of motion of  $\tilde{E}_a^i$ , the gauge constraint (A4), the metric reality conditions (A7), (A8) and the primary condition (A9), we see that (A10) is equivalent to [27]

$$\text{Re}(\mathcal{A}_0^a) = \partial_i(N) \tilde{E}^{ia} + (1/2e) E_i^b N \tilde{E}^{ja} \partial_j \tilde{E}_b^i + N^i \text{Re}(\mathcal{A}_i^a), \quad (\text{A11})$$

or with un-densitized variables,

$$\text{Re}(\mathcal{A}_0^a) = \partial_i(N) E^{ia} + N^i \text{Re}(\mathcal{A}_i^a). \quad (\text{A12})$$

From this expression we see that the secondary triad reality condition restricts the three components of the ‘‘triad lapse’’ vector  $\mathcal{A}_0^a$ . Therefore (A11) is not a restriction on the dynamical variables ( $\tilde{E}_a^i$  and  $\mathcal{A}_i^a$ ) but on the slicing, which we should impose on each hypersurface.

Throughout the discussion in this article, we assume that the initial data of  $(\tilde{E}_a^i, \mathcal{A}_i^a)$  for evolution are solved so as to satisfy all three constraint equations and the metric reality condition (A7) and (A8). Practically, this is obtained, for example, by solving ADM constraints and by transforming a set of initial data to Ashtekar’s notation.

## APPENDIX B: EXPERIMENTS USING THE MAXWELL EQUATION

In this appendix, using the Maxwell equation of the vacuum field, we show that the symmetric hyperbolic system does not change the stability feature drastically. The result here supports the discussion in §V. More detail analysis can be found in our Paper II [41].

The Maxwell equation has two constraint equations,

$$C_E := \partial_i E^i \approx 0, \quad C_B := \partial_i B^i \approx 0, \quad (\text{B1})$$

and two dynamical equations

$$\partial_t E_i = c \epsilon_i^{jk} \partial_j B_k, \quad \partial_t B_i = -c \epsilon_i^{jk} \partial_j E_k \quad (\text{B2})$$

for the field  $(E_i, B_i)$ .

Suppose we have adjusted (B2) using the constraint terms, (B1), with a multiplier,  $\kappa$ .

$$\partial_t E_i = c \epsilon_i^{jk} \partial_j B_k + \kappa_i C_E, \quad \partial_t B_i = -c \epsilon_i^{jk} \partial_j E_k + \kappa_i C_B \quad (\text{B3})$$

where  $\kappa_i = (\kappa, \kappa, \kappa)$  for simplicity. This matrix expression

$$\partial_t \begin{pmatrix} E_i \\ B_i \end{pmatrix} \cong \begin{pmatrix} \delta^{jl} \kappa_i & -c \epsilon_i^{jl} \\ c \epsilon_i^{jl} & \delta^{jl} \kappa_i \end{pmatrix} \partial_l \begin{pmatrix} E_j \\ B_j \end{pmatrix} \quad (\text{B4})$$

immediately tells us its hyperbolicity depending on  $\kappa$  as follows: The system, (B4), becomes symmetric hyperbolic form when  $\kappa = 0$  (that is the original Maxwell equation), becomes weakly hyperbolic form when  $\kappa = \pm c$ , and becomes strongly hyperbolic otherwise. The eigenvalues of the dynamical equation can be written as  $(c, c, -c, -c, \kappa, \kappa)$ .

We made a numerical code to demonstrate a propagation of plane electro-magnetic wave,

$$E^i(x, t) = (0, 0, -\frac{1}{\sqrt{2}} \sin(\frac{x+y}{\sqrt{2}} - ct)), \quad (\text{B5})$$

$$B^i(x, t) = (-\frac{1}{2} \sin(\frac{x+y}{\sqrt{2}} - ct), \frac{1}{2} \sin(\frac{x+y}{\sqrt{2}} - ct), 0) \quad (\text{B6})$$

in 2-dimensional spacetime with periodic boundary condition. We use (B6) as our initial data, and monitor its numerical error during its evolution by evaluating constraint equations. The error itself is quite small, but as we show in Fig.7 we found the difference by a multiplier of the adjusted terms  $\kappa$ . We see that the symmetric hyperbolic equation show the best performance for the stability, but not so much different performance from the strongly hyperbolic system.

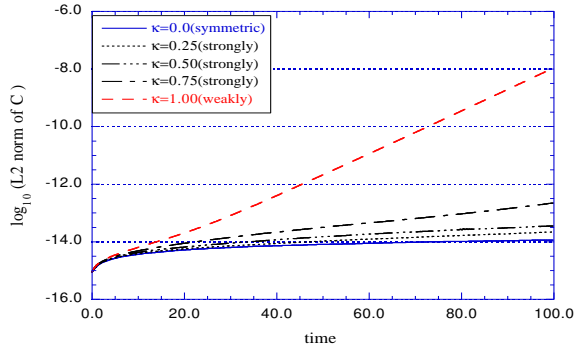


FIG. 7. Comparisons of ‘adjusted’ system with the different multiplier,  $\kappa$ , in eq. (B3). Plots are of L2 norm of the constraint equations, (B1).